NMR as evaluation strategy for cellular uptake of nanoparticles

Tomas Orlando [1,], Alessandro Paolini[2,3], Francesco Pineider[4,5], Emanuela Clementi[3], Francesca Pasi[3], Yannick Guari[6], Joulia Larionova[6], Luciano Sacchi[3], Rosanna Nano[3], Maurizio Corti[1], Alessandro Lascialfari[7,*]*

[1] Department of Physics and INSTM Unit, University of Pavia, Pavia, Italy. [2] Department of Medical Physics, IRCCS Policlinico S. Matteo Foundation, Pavia, Italy. [3] Department of Biology and Biotecnology "Lazzaro Spallanzani", University of Pavia, Pavia, Italy. [4] CNR-ISTM, Padova, Italy. [5] Department of Chemistry and INSTM Unit, University of Florence, Sesto Fiorentino (FI), Italy. [6] Institute Charles Gerhardt Montpellier, CNRS, Chimie Moléculaire et Organisation du Solide, Université Montpellier II, Montpellier, France. [7] Department of Physics and INSTM Unit, Università degli Studi di Milano, Milan, Italy.

Keywords: magnetic nanoparticles, gold nanoparticles, cellular uptake, ^{1}H-NMR, cellular response.

Abstract

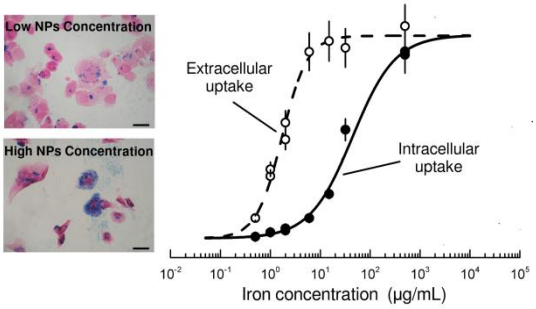

Advanced nanostructured materials, such as gold nanoparticles, magnetic nanoparticles and multifunctional materials, are nowadays used in many state-of-the-art biomedical application. However, although the engineering in this field is very advanced, there remain some fundamental problems involving the interaction mechanisms between nanostructures and cells or tissues. Here we show the potential of ^{1}H-NMR in the investigation of the uptake of two different kinds of nanostructures i.e. maghemite and gold nanoparticles, and of a chemotherapy drug (temozolomide), in glioblastoma tumor cells. The proposed experimental protocol provides a new way to investigate the general problem of cellular uptake for a variety of biocompatible nanostructures and drugs.

The role of nanoscience is currently of primary importance in the development of innovative strategies in the fields of nanomedicine and personalized medicine. Several in vitro studies and pre-clinical trials have been undertaken on a great variety of nanostructures: among these, magnetic nanoparticles and gold nanoparticles represent the core of several advanced biomedical applications. On the one hand, magnetic nanoparticles of novel synthesis can improve the capabilities of already existing and widely used clinical diagnostic and therapeutic techniques[1-3], like e.g. molecular imaging[4-6], magnetic fluid hyperthermia[7] and magnetofection[8], acting as contrast agents, markers and carriers respectively. Moreover, the possibility of new approaches to synthesize a single nanostructure with more than one function[9-11] gives the opportunity to

overcome the limitations of standard medicine. On the other hand, gold nanoparticles are used in several biomedical applications: due to their versatility, their physical properties and the easy synthesis procedure, functionalized gold nanoparticles play an important role in some advanced antitumor therapies, allowing an enhancement of X-ray radiation cross section (useful in radiotherapy and in CT diagnosis) or improving drug solubility[11-13].

Despite the great amount of scientific research produced during the last 10 years in the field of magnetic and metallic nanoparticles, concerning in particular engineering and design characteristics of nanostructures[15-18], there are still some critical points regarding basic aspects of the interaction between exogenous nanostructures and biological systems[19]; indeed, the cell uptake of nanoparticles after their injection into the circulation is of primary importance, the clinical *in vivo* application being the final goal of these researches. Although some experimental techniques such as fluorescence microscopy and electron microscopy can supply qualitative information about the uptake mechanisms, very few techniques can provide reliable and quantitative information about the mechanisms of uptake on a great variety of samples and biological systems[22,38,39].

In order to better understand the basic cellular uptake mechanisms at a microscopic level, we developed a versatile method based on broadband ^{1}H-NMR to study the *in vitro* cellular response as a function of concentration of external agents. Indeed, ^{1}H-NMR relaxometry experiments allow to measure two characteristic parameters related to the relaxation process of the hydrogen nuclear magnetization, i.e. the longitudinal relaxation time T_1 and the transverse relaxation time T_2. Given that these quantities depend on the interaction between the hydrogen nuclei (protons) and the surrounding spins and lattice, they give information about the microscopic properties of the sample. We tested the potential for the experimental setup using different kinds of exogenous

biocompatible agents, i.e. magnetic nanoparticles, gold nanoparticles and an antitumor drug (temozolomide), proving that this method could represent a new way to obtain quantitative information on a wide variety of uptake phenomena. Furthermore, in order to check the experimental efficacy of such a protocol on different biological systems, two different human glioblastoma immortalized cell lines were selected, i.e. T98G and U251. The choice of these cell lines was strongly supported by the great interest of the scientific community in developing more effective therapies (and alternatives to surgery) against such form of very aggressive brain cancer[20,21].

Magnetic nanoparticles (MNPs). Rhamnose-coated (magnetic core diameter = 18.2 ± 1.1 nm) iron oxide MNPs were used. As demonstrated in Ref. 22, they resulted as good contrast agents for Magnetic Resonance Imaging (MRI), displaying a nuclear transverse relaxivity as high as 300 $s^{-1}mM^{-1}$ at 20 MHz, and good Magnetic Fluid Hyperthermia (MFH) agents, having a specific absorption rate (SAR) value greater than 60 W/g. Furthermore, the stability of MNPs in water solution was proved by DLS and TEM measurements in Ref. 22; this is allow us to exclude any a priori aggregation contribution to the cellular uptake[37]. In both techniques, an evaluation of the degree of cellular uptake is crucial for diagnostic and therapeutic purposes.

After incubating the MNPs with the two different glioblastoma cell lines for 24 hours, we carried out experiments of intra-cellular localization by optical microscopy (Figure 1); indeed, by means of the Prussian Blue reaction, MNPs can be easily recognized. The results show a marked tendency by both cell lines to capture the nanoparticles, with a great phagocytic activity even at low concentrations (i.e. 2 μg/mL). Furthermore, it can be observed that MNPs are only found in the cytoplasm, while they are completely absent in the nucleus. A relevant increase of cellular dimensions closely correlated to the concentration of nanoparticles can also be observed.

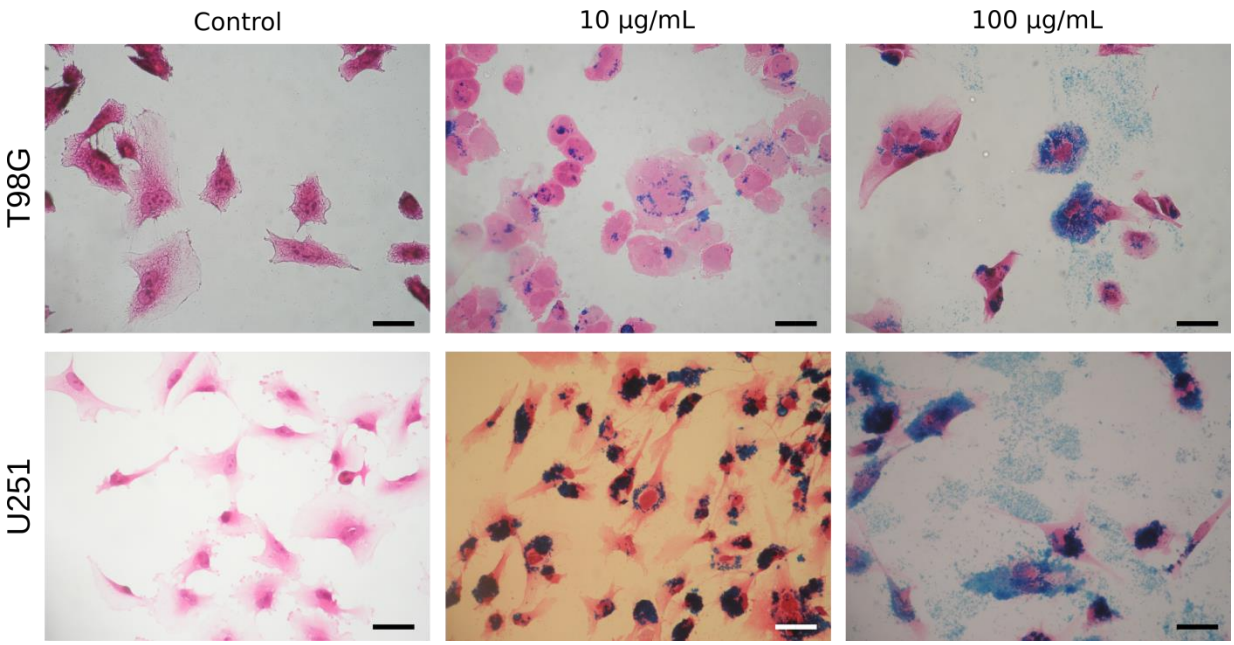

Figure 1. Optical images of human glioblastoma cells (T98G and U251) after 24 h of incubation with rhamnose-coated MNPs as a function of iron concentration in the culture medium (scale bars = 20 µm).

In order to confirm the presence of nanoparticles inside the cells, Transmission Electron Microscopy (TEM) images were taken (Figure 2). These images show how nanoparticles and the plasma membrane interact: indeed, MNPs are observed both on the membrane surface (Figure 2a) and, after internalization, in lysosomes (Figure 2b). The cell membrane invaginations and vacuole formation are indicative of endocytosis, whereas the membrane extrusions are connected to phagocytosis. The high number of these membrane modifications confirms the strong tendency of the cells to capture MNPs. These are localized under membrane ruffles and in internalized vesicles (Figure 2c). MNPs concentrated in cytoplasmic vesicles do not have any

precise compartmentalization. These vesicles migrated to the perinuclear region and fused with

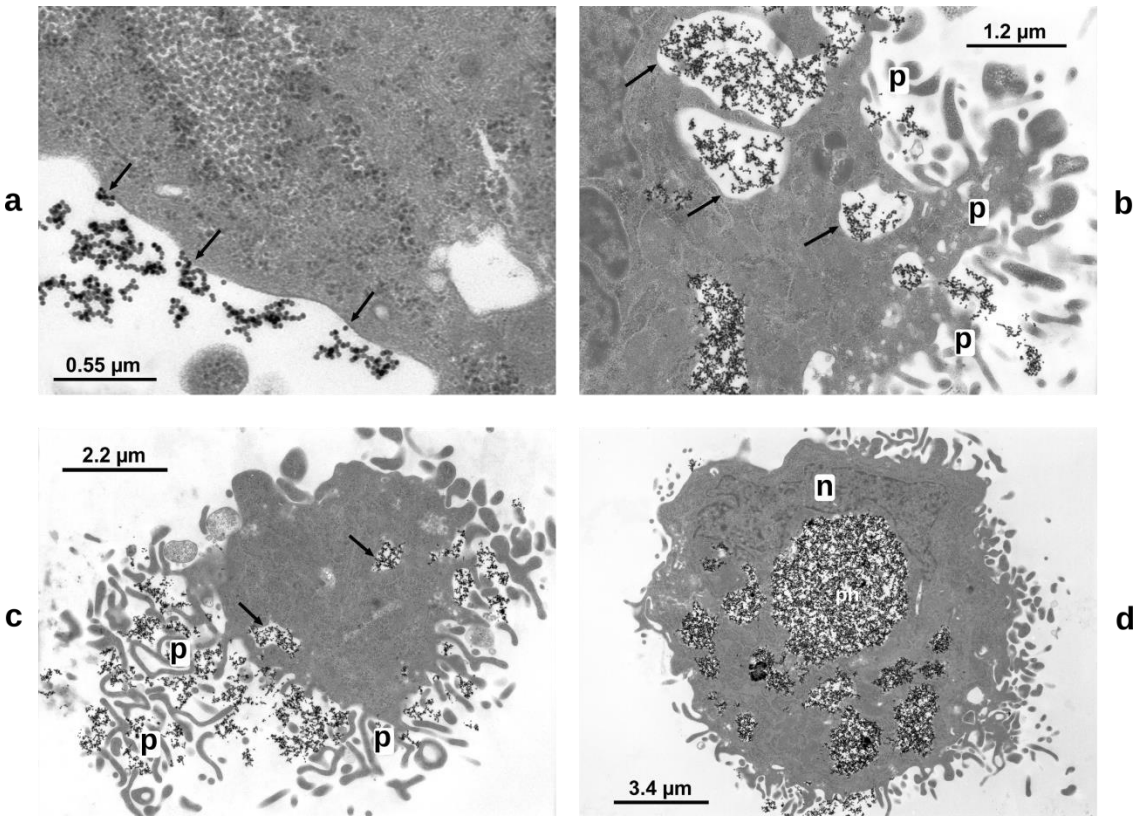

other vesicles forming larger phagosomes (Figure 2d). This phenomenon is particularly evident

Figure 2. TEM images of T98G cells at $C_{[Fe]}$ = 25 µg/mL. MNPs can be localized in different positions: attached on plasma membrane (a), internalized by pseudopodia, p, or incorporated into phagosomes, arrows (b). Note the high number of pseudopodia, p, indicating the strong tendency of the cell to capture MNPs (c). The vesicles in the perinucleal region (n = nucleus) are fused forming larger phagosomes (d). Similar considerations are valid for U251 cell line (see Supplementary Information).

at high concentrations of nanoparticles.

To study quantitatively the uptake of MNPs and to disclose the mechanisms of MNP-cell interactions, a broad-band ^{1}H-NMR investigation was performed[23]. We chose 20 MHz as working frequency, reaching a good compromise between sensitivity (i.e. signal intensity) and easiness of the method, being 20 MHz the typical frequency of commercial largely available bench-top NMR spectrometers. Using a step by step optimization, we were able to achieve a preparation protocol that allowed us to obtain *in vitro* samples suitable for NMR measurements. At the end of the process, the cells are well dispersed in a liquid matrix and the samples are homogeneous. Several different iron concentrations were used, covering the range 0.5 μg/mL - 500 μg/mL. ^{1}H-NMR transversal (T_2) nuclear relaxation time was measured beginning with the first acquisition at 2 hours from sample preparation and concluding the protocol within a few hours, in order to avoid cell death and sample deterioration. In this way, even if all the measurements were performed at room temperature, we can consider the cells alive throughout the experiment's short duration (see Supporting Information for details).

The effect of different concentrations of MNPs in the measured *in vitro* samples has been studied by investigating the relaxation curve of the transverse nuclear magnetization, due to the great sensitivity of this mechanism to the local inhomogeneities with respect to the relaxation of the longitudinal component of the nuclear relaxation. In a water solution the transverse decay is described by a single exponential behaviour with a time constant T_2. In the present case, a more complex behaviour was observed: two different contributions to the nuclear transverse relaxation curve were observed, a "T_2 fast component" ($T_{2,FAST}$) and a "T_2 slow component" ($T_{2,SLOW}$), clearly distinguished according to T_2 length (see insets of Figure 3a and 3b). As can be noticed

by looking at Table 1, the absolute values of these two components differ by approximately one order of magnitude, both for T98G and U251. The values of the relaxation rates $1/T_{2,FAST}$ and $1/T_{2,SLOW}$ as a function of MNPs iron concentration ($C_{[Fe]}$) are shown in Figure

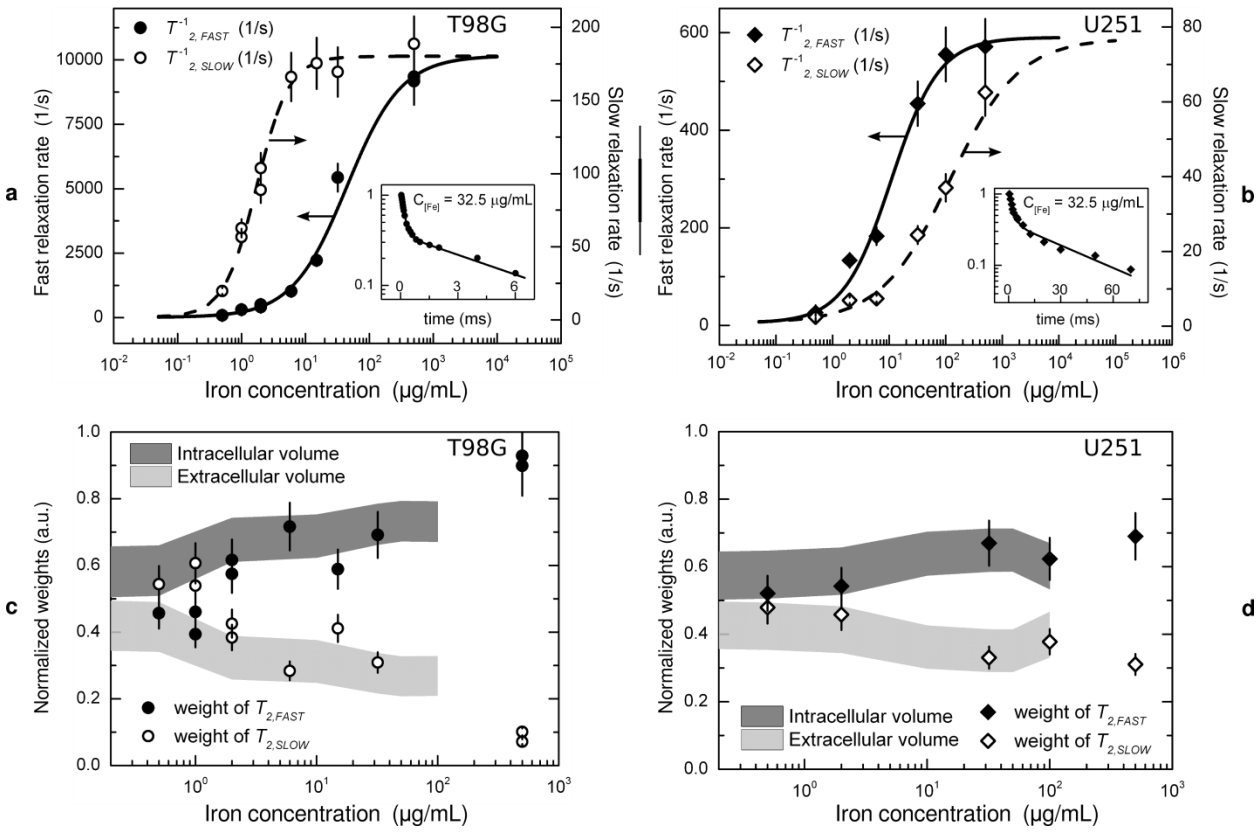

Figure 3. ^{1}H-NMR data and volume evaluations as a function of iron concentration. Fast (●,◆) and slow (○,◇) transverse relaxation rates for T98G (a) and U251 (b) cells as a function of iron concentration ($C_{[Fe]}$) are shown. The fits were performed using a logistic function (Eq. 1). The insets in (a) and (b) show two typical decay curves normalized to 1 in semi-logarithmic scale: the bi-exponential behaviour is clearly visible. Relative normalized weights of T_2 fast and slow components as a function of $C_{[Fe]}$ for T98G (c) and U251 (d) are also shown (●,○ and ◆,◇ respectively). The error was quantified as 10% for both T_2 and weights values (see Supplementary Information for details). The centre of the colored bands represents the intra-cellular and the extra-cellular volumes calculated on the basis of the average diameter estimated with optical microscopy. The bandwidth corresponds to the experimental error.

Table 1 | Transverse relaxation times and dose-response fit results*.

		$T_{2,FAST}$	$T_{2,SLOW}$
T98G	Values (ms)	0.1 ÷ 11.5	5.5 ÷ 51.0
	EC50	44 ± 17	1.7 ± 0.1
	p	1.02 ± 0.08	1.7 ± 0.1
U251	Values (ms)	1.7 ÷ 30.0	16.0 ÷ 300.0
	EC50	10 ± 5	117 ± 40
	p	1.0 ± 0.1	0.71 ± 0.07

* The quality of the fit is confirmed by $\overline{R}^2$ values, always greater than 0.93.

3a and 3b for T98G and U251 cell lines respectively. In Figure 3c and 3d we report the normalized relative weights of $T_{2,FAST}$ and $T_{2,SLOW}$ components.

By a simultaneous analysis of microscope images, both optical and electronic, and NMR results, it was possible to identify the proton groups giving rise to different T_2 components as belonging to different biological environments. To do this, we recall that in MRI *in vivo* images of brain a multi-exponential analysis of the T_2 relaxation curves allowed the contribution of slowly relaxing "free protons" (coming from extra-cellular water) to be separated from that of fast relaxing "not-free protons" (pertaining to intra-cellular water)[24,25]. Following this distinction, the slow relaxing component ($1/T_{2,SLOW}$) can be attributed to "free protons" of bulk water in direct contact only with MNPs on the cells membrane surface or at the beginning of the phagocytosis process. On the other hand, the fast relaxing component ($1/T_{2,FAST}$) can be associated with the intra-cellular environment, i.e. to the "not-free protons" (that is with limited motion) of intra-cellular water and of MNP coating. Given that the T_2 value is inversely proportional to the superparamagnetic particle concentration[26], we can assume that $T_{2,FAST}$ and $T_{2,SLOW}$ are indirect measurements of the amount of MNPs in the intra-cellular and in the extra-cellular environment, respectively.

In order to quantify the degree of uptake as a function of $C_{[Fe]}$, our data were fitted by a logistic curve, a well-known model commonly used in physiological and pharmacological studies to investigate the dose-response behaviour of hormones, drugs and neurotransmitters[27]. In our case, it takes the following analytical form:

$$\frac{1}{T_2} = \left(\frac{1}{T_2}\right)_{\max} + \frac{\left(\frac{1}{T_2}\right)_{control} - \left(\frac{1}{T_2}\right)_{\max}}{1 + \left(\frac{C_{[Fe]}}{EC50}\right)^{p}} \qquad (1)$$

where 1/T2 is the "response" and C[Fe] is the "dose". The parameter (1/T2)control represents the blank response and it was fixed equal to the experimental value measured for the control sample (i.e. with no MNPs incubation); (1/T2)max is the saturation response value and it was chosen near the 1/T2 experimental value for C[Fe] = 500 μg/mL. The quantity p is the slope factor, which gives the maximum slope of the curve, while EC50 is the half maximal effective concentration. The values obtained from the fit procedure are shown in Table 1. Despite the wide range of concentrations (almost five orders of magnitude), the logistic fit performed on the NMR data worked well, as seen in Figure 3a and 3b. This is further evidence of the fact that rhamnose-coated iron-oxide NPs are internalized by cells through an active mechanism, as explained below. Indeed, one has to observe that, since the logistic model is typical of agonist/receptor interactions[28-30], its applicability to this case could be an indirect indication of receptor-mediated endocytosis or phagocytosis. In particular, the uptake mechanism of these two glioblastoma cell lines is similar to that of macrophages and the massive presence of long pseudopodia leads us to hypothesize a phagocytosis by carbohydrate-binding proteins, such as lectins, strongly involved in cancer communications[31].

From a quantitative point of view, the NMR results confirm the great phagocytic activity already highlighted by optical and TEM images. Indeed, the internalization process does not stop until very high concentrations, as demonstrated for both the cell lines (T98G and U251) by $1/T_{2,FAST}$ maximum value, which is reached only for high iron concentrations ($C_{[Fe]}$ > 100 μg/mL). Furthermore, by comparing EC50 values evaluated from $T_{2,FAST}$ curves, we gather that U251 cells show a more rapid internalization in respect to T98G ($EC50_{T98G} > EC50_{U251}$ for $T_{2,FAST}$). As a consequence, $1/T_{2,SLOW}$ of U251 cells increases more slowly than the one of T98G cells, confirming the fact that, in this cell line, at low and intermediate concentrations, few MNPs remain in the extra-cellular environment.

Finally, by increasing the MNP concentration, the weight of the $T_{2,FAST}$ component increases, while the one of $T_{2,SLOW}$ diminishes (Figure 3c and 3d), indicating a rising amount of intra-cellular water. This evidence of a turgor pressure enhancement, probably due to cellular swelling, is confirmed by a simple statistical analysis which shows an increase in average cell diameter (+28% for T98G and +14% for U251 at 50 μg/mL) as a function of concentration. The intra-cellular and extra-cellular volumes can be estimated using cell diameter data (see Summary Methods for details): the quantitative agreement between these estimations and the changes of the relative weight of fast and slow T_2 components can be seen in Figure 3c and 3d.

Gold nanoparticles (GNPs). The ability to obtain information on the uptake process using broadband ^{1}H-NMR was then tested on in vitro samples incubated with non-magnetic nanostructures. Considering the great interest in metallic nanoparticles and their wide use in

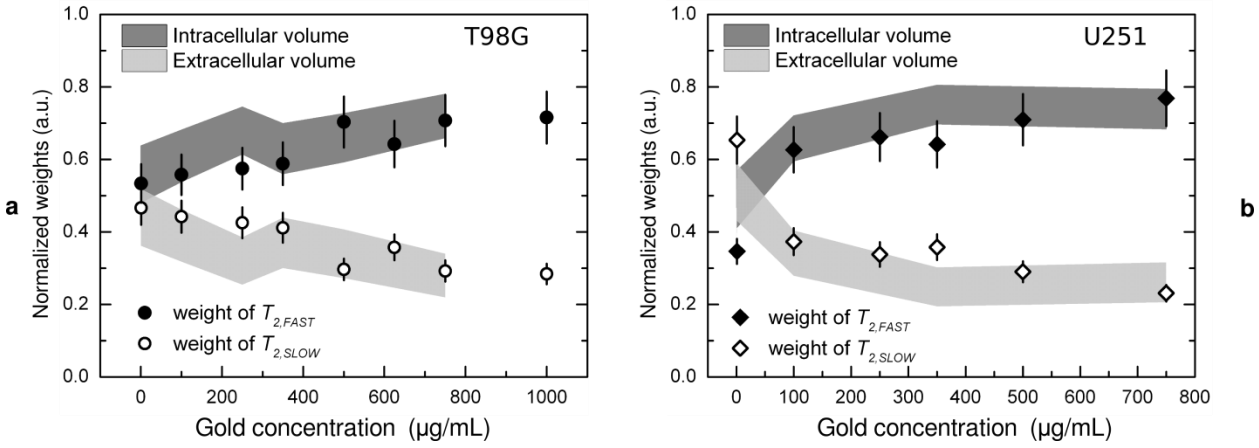

Figure 4. ^{1}H-NMR data and volume evaluations as a function of gold concentration. NMR weights of the two T_2 components, fast and slow, are shown for (a) T98G (● and ○ respectively) and (b) U251 (◆ and ◇ respectively). The volume evaluations obtained with optical microscopy are shown as colored bands, grey for intra-cellular volume and red for the extra-cellular one. The bandwidth corresponds to the experimental error.

biomedical application as e.g. sensors, we chose fully biocompatible gold nanoparticles (metallic core = 16.7 ± 1.6 nm) coated with sodium citrate[32].

Optical microscopy was performed on glioblastoma cells (both T98G and U251) after 24 hours of incubation with GNPs (images reported in Supplementary Information) and the average diameter was evaluated for different gold concentrations. As observed for MNPs, these experiments show an intra-cellular distribution at cytoplasmic level for both cell lines, without significant differences. In order to obtain in vitro samples suitable for NMR measurements, the same preparation procedure adopted for MNPs was used for GNPs. The range of concentrations explored covers almost three orders of magnitude, going from 1 µg/mL to 750 µg/mL (1000 µg/mL for T98G). Two different transverse nuclear relaxation times, i.e. $T_{2,FAST}$ and $T_{2,SLOW}$,

were measured. Using the previous arguments, they can be associated with the intra-cellular and with the extra-cellular environment respectively. The weights of the two T_2 components, normalized with respect to the total signal intensity, are reported in Figure 4. The volume percentages of intra- and extra-cellular volumes calculated starting from the average diameter estimated with optical microscopy are also shown. As can be seen, the agreement between the data obtained with two different techniques (NMR and optical microscopy) is fully within the error, proving once more the capability of ^{1}H-NMR to probe the sample at a microscopic level.

In the case of GNPs, a quantitative estimation of the T_2 evolution as a function of gold concentration $C_{[Au]}$ will require a future detailed investigation, due to the gold diamagnetism, whose influence on T_2 is still not well understood. The stimulated response of the system (by the presence of GNPs) is reflected by the behaviour of the relative weights of the two components. An increase in intra-cellular weight with increasing Au concentration can be observed for both cell lines, indicating cellular swelling (volume increase), possibly due to the cellular stress induced by GNP phagocytosis. In particular, T98G cell line weights of T_2 components are characterized by a monotonic variation over the whole range of concentrations $C_{[Au]}$, while U251 exhibit a more rapid increase at very low $C_{[Au]}$ (< 100 μg/mL) followed by a plateau. This observation confirms a faster internalization process for U251 cells with respect to T98G, as already proved in the MNPs case.

Temozolomide (TMZ). Additional experiments on the same apparatus were performed on glioblastoma cells incubated with temozolomide (TMZ), a specific antitumor drug which has the ability to pass through the blood-brain barrier[33,34]. TMZ has a cytotoxic effect caused by the methylation of the O^6 position of guanine, which causes a DNA double-strand break and initialization of an apoptosis pathway[35]. In accordance with standard treatment protocols, the

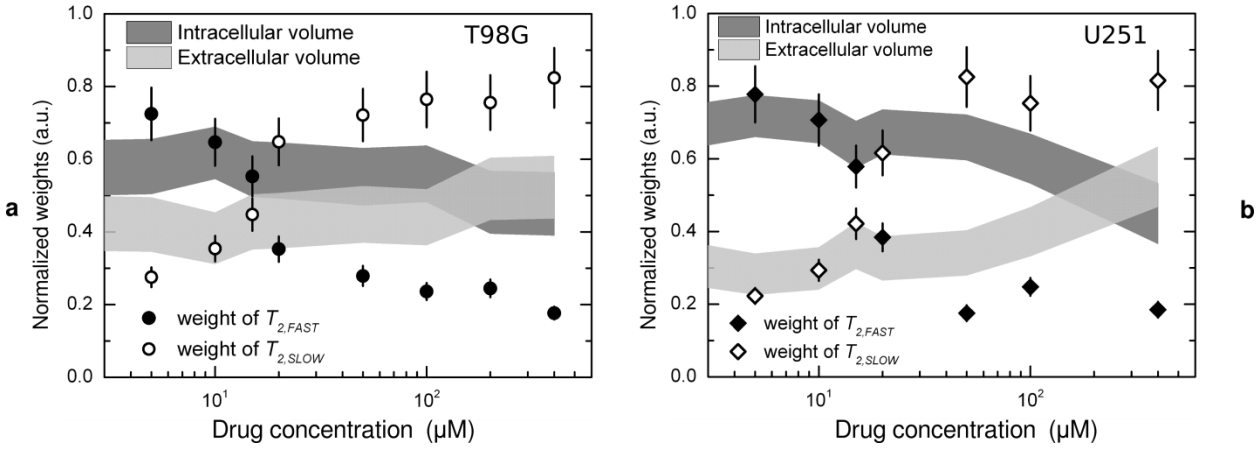

Figure 5. ^{1}H-NMR data and volume evaluations as a function of temozolomide concentration. NMR weights of the two T_2 components, fast and slow, are shown for (a) T98G (● and ○ respectively) and (b) U251 (◆ and ◇ respectively). The volume evaluations obtained with optical microscopy are shown as colored bands, grey for intra-cellular volume and red for extra-cellular one. The bandwidth corresponds to the experimental error.

cells cultures (T98G and U251) were incubated with TMZ for two hours. After this short period the samples were measured by ^{1}H-NMR within a few hours, in order to avoid extra toxicity effects due to the extended action of the drug. A wide range of concentrations was explored, starting from 5 μM to 400 μM: the dose indicated by common in vitro treatment plans is 20 μM.

Also in this case, ^{1}H-NMR is able to distinguish between the fast relaxing signal ($T_{2,FAST}$) coming from intra-cellular protons and the slow relaxing signal ($T_{2,SLOW}$) from extra-cellular protons. The weight of each component gives a quantitative estimation of the amount of protons in each biological environment (i.e. intra- and extra-cellular). They are reported in Figure 5 for

T98G and U251 cell lines, together with an estimation of the volumes obtained from the optical microscopy measurements of diameter.

Instead of a monotonic behaviour of the weights as a function of concentration of MNPs and GNPs, some anomalous features can be observed when cells are treated with TMZ. In particular, for very low drug doses, i.e. $C_{[TMZ]} < 10$ μM, an increase in intra-cellular weights for both T98G and U251 is observed, confirmed by optical microscopy data. This behaviour is an indication of autophagy, a stress reaction caused by TMZ that induces cellular turgor[36], but still compatible with cell alive. By increasing the drug dose in the range 10 μM $< C_{[TMZ]} <$ 30 μM, a fast decrease of the intra-cellular weight for both cell lines can be noticed. This decreasing trend is only partially confirmed by the volume reduction detected by means of optical microscopy. Actually, an important gap among the percent weights and volumes opens up around the common treatment dose, i.e. 20 μM. This discrepancy can be explained by considering that during the incubation time, a fraction of cells dies by apoptosis and detach easily from the plate. These cells are then washed away during the sample preparation and do not contribute to the intra-cellular NMR signal. On the other hand, optical microscopy evaluates the cell diameter, but is not sensitive to the total number of cells.

For very high doses ($C_{[TMZ]} > 50$ μM), the NMR weights reach a sort of plateau, confirming that the killing action of the drug is complete. By considering the value of the gap between NMR percent weights and volumes estimated by microscopy, the fraction of dead cells can be quantified as 30% for T98G and 40-45% for U251. A decrease of the cells diameter as a function of concentration is still visible. This observation reveals that the surviving cells are close to apoptosis, the shrinkage being a common effect of this process[40].

In summary, ^{1}H-NMR revealed itself as a powerful tool to investigate the microscopic properties of *in vitro* cell cultures in presence of exogenous nanostructures, having the capability to probe both the intra- and extra-cellular ^{1}H-based environment. We studied the response of two different glioblastoma cell lines exposed to three different exogenous agents, i.e. magnetic nanoparticles, gold nanoparticles and an antitumor drug, following the phenomena over a wide range of concentration (at least three orders of magnitude).

By evaluating the transverse nuclear relaxation times, we demonstrated the existence of an uptake law for rhamnose coated iron-oxide MNPs in human glioblastoma tumor cells. Furthermore, cell swelling and cell death can be easily investigated as a function of concentration when external agents of different nature (magnetic nanoparticles, metallic nanoparticles, drugs) are incubated with cells. The presented experiment could be considered an innovative method and represent a new general strategy to improve the knowledge of the uptake process and of the intra- and/or extra- cellular localization of a variety of nanostructured compounds.

Methods Summary. To investigate the cellular uptake of MNPs, we chose rhamnose-coated iron-oxide nanoparticles[22] as an efficient bifunctional targeting system for theranostic applications, because of the high MRI contrast efficiency, the good magnetic hyperthermia effect and the marked tendency of the rhamnose coating to target skin tumours. These nanoparticles are also biocompatible and non-toxic. The magnetic core, made of magnetite (Fe_3O_4), has a spherical geometry with a diameter of 18.2 ± 1.1 nm (TEM characterization), while the hydrodynamic diameter for the whole nanoparticle is 23 nm. All these details are reported in Ref. 16. Citrate-capped gold nanoparticles were prepared using a modified version of the standard Turkevich method[32]; the mean size of the spherical particles is 16.7 ± 1.6 nm, as estimated by TEM

imaging. As biological systems, we used two kinds of human glioblastoma immortalized cell lines, i.e. T98G and U251.

The incubation of such cells with MNPs was performed in a plate and the experimental observations allowed us to exclude any sedimentation effects on the cellular uptake process[37]. Optical and TEM images were acquired using standard protocols and instruments: the details are given in the Supplementary Information. Using optical microscopy images, the average cell diameter (± 0.5 μm) was estimated for different MNPs, GNPs and TMZ concentrations.

In order to obtain in vitro samples suitable for NMR measurements, an original sample preparation protocol was developed. After the incubation time with the external agent (24 h for MNPs and GNPs, 2 h for TMZ), several washings and centrifugations were performed and a cellular pellet without free (not absorbed) nanoparticles and other impurities (like dead cells) that could give rise to spurious NMR signals was obtained. Then, at the end of the preparation, 10 μL of clean culture medium was added.

The evaluation of the intra-cellular volume in the NMR sample was calculated as follows, using average cell diameters data: (Single Cell Volume) × (Number of Cells), where the number of cells is $5 \cdot 10^6$ for T98G and $4 \cdot 10^6$ for U251, taking into account their different growth rates. The extra-cellular volume was quantified as 10 μL + 5 μL, considering the clean culture medium added at the end of the preparation and a reasonable experimental error.

ASSOCIATED CONTENT

Supporting Information.

Complete optical microscopy images, cellular diameter evaluation, TEM images for U251 cell line, viability experiments, NMR setup details, complete NMR data and fit results. This material is available free of charge via the Internet at http://pubs.acs.org.

AUTHOR INFORMATION

Corresponding Author

*tomas.orlando@unipv.it, alessandro.lascialfari@unimi.it.

Author Contributions

The manuscript was written through contributions of all authors. All authors have given approval to the final version of the manuscript. T.O. and A.P. contributed equally.

ACKNOWLEDGMENT

Financial support was partly provided by the FIRB projects RINAME no. RBAP114AMK, INSTM-Regione Lombardia MAG-NANO and Rete ItalNanoNet no. RBPR05JH2P. We thank L. Cattaneo for technical support in the development of the NMR setup, L. Lartigue and M.P. Conte for the help in the synthesis of magnetic nanoparticles, and M. Mariani for helpful discussions.

REFERENCES

1. Pankhurst, Q.; Thanh, N.; Jones, S.; Dobson, J. *J. Phys. D. Appl. Phys.* **2009**, *42*, 224001.
2. Davis, M. E.; Chen, Z. G.; Shin, D. M. *Nat. Rev. Drug Discov.* **2008**, *7*, 771–782.
3. Roca, a G.; Costo, R.; Rebolledo, a F.; Veintemillas-Verdaguer, S.; Tartaj, P.; González-Carreño, T.; Morales, M. P.; Serna, C. J. *J. Phys. D. Appl. Phys.* **2009**, *42*, 224002.
4. Flacke, S.; Fischer, S.; Scott, M. J.; Fuhrhop, R. J.; Allen, J. S.; McLean, M.; Winter, P.; Sicard, G. A.; Gaffney, P. J.; Wickline, S. A.; Lanza, G. M. *Circulation* **2001**, *104*, 1280–1285.
5. Massoud, T. F.; Gambhir, S. S. *Genes Dev.* **2003**, *17*, 545–580.
6. Ghosh, D.; Lee, Y.; Thomas, S.; Kohli, A. G.; Yun, D. S.; Belcher, A. M.; Kelly, K. A. *Nat. Nanotechnol.* **2012**, *7*, 677–682.
7. Jordan, A.; Scholz, R.; Maier-Hauff, K.; Johannsen, M.; Wust, P.; Nadobny, J.; Shirra, H.; Schmidt, H.; Deger, S.; Loening, S.; Lanksch, W.; Felix, R. *J. Magn. Magn. Mater.* **2001**, *225*, 118–126.
8. Scherer, F.; Anton, M.; Schillinger, U.; Henke, J.; Bergemann, C.; Kruger, A.; Gansbacher, B.; Plank, C. *Gene Ther.* **2002**, *9*, 102–109.
9. Berry, C. C. *J. Phys. D. Appl. Phys.* **2009**, *42*, 224003.
10. Janib, S. M.; Moses, A. S.; MacKay, J. A. *Adv. Drug Deliv. Rev.* **2010**, *62*, 1052–1063.
11. Lu, C.-W.; Hung, Y.; Hsiao, J.-K.; Yao, M.; Chung, T.-H.; Lin, Y.-S.; Wu, S.-H.; Hsu, S.-C.; Liu, H.-M.; Mou, C.-Y.; Yang, C.-S.; Huang, D.-M.; Chen, Y.-C. *Nano Lett.* **2007**, *7*, 149–154.
12. Dreaden, E. C.; Alkilany, A. M.; Huang, X.; Murphy, C. J.; El-Sayed, M. A. *Chem. Soc. Rev.* **2012**, *41*, 2740–2779.

13. Dreaden, E. C.; Mwakwari, S. C.; Sodji, Q. H.; Oyelere, A. K.; El-Sayed, M. a. *Bioconjug. Chem.* **2009**, *20*, 2247–2253.

14. Alvarez, Y. D.; Fauerbach, J. a; Pellegrotti, J. V; Jovin, T. M.; Jares-Erijman, E. A; Stefani, F. D. *Nano Lett.* **2013**, *13*, 6156–6163.

15. Arosio, P.; Thévenot, J.; Orlando, T.; Orsini, F.; Corti, M.; Mariani, M.; Bordonali, L.; Innocenti, C.; Sangregorio, C.; Oliveira, H.; Lecommandoux, S.; Lascialfari, A.; Sandre, O. *J. Mater. Chem. B* **2013**, *1*, 5317.

16. Jiang, W.; Kim, B. Y. S.; Rutka, J. T.; Chan, W. C. W. *Nat. Nanotechnol.* **2008**, *3*, 145–150.

17. Haick, H. *J. Phys. D. Appl. Phys.* **2007**, *40*, 7173–7186.

18. Chithrani, B. D.; Ghazani, A. A; Chan, W. C. W. *Nano Lett.* **2006**, *6*, 662–668.

19. Albanese, A.; Tang, P. S.; Chan, W. C. W. *Annu. Rev. Biomed. Eng.* **2012**, *14*, 1–16.

20. Adamson, C.; Kanu, O. O.; Mehta, A. I.; Di, C.; Lin, N.; Mattox, A. K.; Bigner, D. D. *Expert Opin. Investig. Drugs* **2009**, *18*, 1061–1083.

21. Nano, R; Lascialfari, A.; Corti, M.; Paolini, A.; Pasi, F.; Corbella, F.; Di Liberto, R. *Anticancer Res.* **2012**, *32*, 2755-2758.

22. Lartigue, L.; Innocenti, C.; Kalaivani, T.; Awwad, A.; Sanchez Duque, M. D. M.; Guari, Y.; Larionova, J.; Guérin, C.; Montero, J.-L. G.; Barragan-Montero, V.; Arosio, P.; Lascialfari, A.; Gatteschi, D.; Sangregorio, C. *J. Am. Chem. Soc.* **2011**, *133*, 10459–10472.

23. Lee, H.; Sun, E.; Ham, D.; Weissleder, R. *Nat. Med.* **2008**, *14*, 869–874.

24. Whittall, K. P.; Mackay, A. L.; Graeb, D. A.; Nugent, R. A.; Li, D. K.; Paty, D. W. *Magn. Reson. Med.* **1997**, *37*, 34–43.

25. Lascialfari, A.; Zucca, I.; Asdente, M.; Cimino, M.; Guerrini, U.; Paoletti, R.; Tremoli, E.; Lorusso, V.; Sironi, L. *Magn. Reson. Med.* **2005**, *53*, 1326–1332.

26. Roch, A.; Muller, R. N.; Gillis, P. *J. Chem. Phys.* **1999**, *110*, 5403–5411.

27. DeLean, A.; Munson, P.; Rodbard, D. *Am. J. Physiol.* **1978**, *235*, E97–102.

28. Arrang, J.; Garbarg, M.; Lancelo, J.; Lecomte, J.; Pollard, H.; Robba, M.; Schunack, W.; Schwartz, J. *Nature* **1987**, *327*, 117–123.

29. Kenakin, T. *Trends Pharmacol. Sci.* **1995**, *16*, 188–192.

30. Chambers, J.; Ames, R. S.; Bergsma, D.; Muir, A.; Fitzgerald, L. R.; Hervieus, G.; Dytko, G. M.; Foley, J. J.; Martin, J.; Liu, W.; Park, J.; Ellis, C.; Ganguly, S.; Konchar, S.; Cluderay, J.; Leslie, R.; Wilson, S.; Sarau, H. M. *Nature* **1999**, *400*, 261–265.

31. Nangia-Makker, P.; Conklin, J.; Hogan, V.; Raz, A. *Trends Mol. Med.* **2002**, *8*, 187–192.

32. Kimling, J.; Maier, M.; Okenve, B.; Kotaidis, V.; Ballot, H.; Plech, A. *J. Phys. Chem. B* **2006**, *110*, 15700–15707.

33. Spiegl-Kreinecker, S.; Pirker, C.; Marosi, C.; Buchroithner, J.; Pichler, J.; Silye, R.; Fischer, J.; Micksche, M.; Berger, W. *Br. J. Cancer* **2007**, *96*, 960–969.

34. DeAngelis, L. M. *Sem. Onc.*, **2003**, *30*, 15-18.

35. Robinson, C. G.; Palomo, J. M.; Rahmathulla, G.; McGraw, M.; Donze, J.; Liu, L.; Vogelbaum, M. A. *Br. J. Cancer* **2010**, *103*, 498–504.

36. Kanzawa, T.; Germano, I. M.; Komata, T.; Ito, H.; Kondo, Y.; Kondo, S. *Cell Death Differ.* **2004**, *11*, 448–457.

37. Cho, E. C.; Zhang, Q.; Xia, Y. *Nat. Nanotechnol.* **2011**, *6*, 385–391.

38. Semmling, M.; Kreft, O.; Muñoz Javier, A.; Sukhorukov, G. B.; Käs, J.; Parak, W. J. *Small* **2008**, 4, 1763–1768.

39. Zhang,F.; Lees, E.; Amin, F.; Rivera Gil, P.; Yang, F.; Mulvaney, P.; Parak, W. J. *Small* **2011**, 7, 3113–3127.

40. Kerr, J.; Wyllie, A.; Currie, A. *Br. J. Cancer* **1972**, 26, 239–257.